Importance of Matrix Elements in the ARPES Spectra of BISCO

A. Bansil[1] and M. Lindroos[1,2]
[1]*Physics Department, Northeastern University, Boston, Massachusetts 02115*
[2]*Tampere University of Technology, P.O. Box 692, FIN-33101 Tampere, Finland*
(Received 9 July 1999)

We have carried out extensive first-principles angle-resolved photointensity (ARPES) simulations in Bi2212 wherein the photoemission process is modeled realistically by taking into account the full crystal wave functions of the initial and final states in the presence of the surface. The spectral weight of the ARPES feature associated with the CuO_2 plane bands is found to undergo large and systematic variations with $k_\parallel$ as well as the energy and polarization of the incident photons. These theoretical predictions are in good accord with the corresponding measurements, indicating that the remarkable observed changes in the spectral weights in Bi2212 are essentially a matrix element effect and that the importance of matrix elements should be kept in mind in analyzing the ARPES spectra in the high T_c's.

PACS numbers: 79.60.Bm, 71.18.+y, 74.72.Hs

Angle-resolved photoemission spectroscopy (ARPES) has contributed significantly towards an understanding of the nature of the normal as well as the superconducting state of the cuprates [1–4]. Much of the data on the cuprates, however, have been analyzed by assuming that the ARPES essentially measures the one-particle spectral function of the initial states. While this simple approach yields insights into the underlying physics, a satisfactory description of the spectra must necessarily model the photoexcitation process properly by taking into account the matrix element involved, the complex modifications of the wave functions resulting from a specific surface termination, and the effects of multiple scattering and of finite lifetimes of the initial and final states.

This article presents first-principles simulations of ARPES spectra in Bi2212 (BISCO) using the one-step model of photoemission which incorporates the aforementioned effects realistically [5–10]. We focus on the ARPES signature of CuO_2 plane bands which are widely believed to be the key to the mechanism of superconductivity in the cuprates. The spectral weight of the ARPES peak associated with the CuO_2 plane bands is found to undergo large variations with $\mathbf{k}_\parallel$ as well as the energy and polarization of the incident photons. These theoretical predictions are in remarkable accord with the corresponding measurements [11] on BISCO, and show clearly the importance of "matrix element effects" [12] in the ARPES spectra. Notably, a substantial increase in the ARPES spectral weight in BISCO in going from $\overline{\Gamma}$ to $\overline{M}$ was noted early by Anderson [13], who speculated that this puzzling behavior may be the hallmark of spin charge separation.

The physical and formal underpinnings of our approach may be exposed by starting with the following golden-rule–based expression for photointensity from initial states at energy E with photons of energy $\hbar\omega$ [14]:

$$I(E,\hbar\omega) = \frac{2\pi e}{\hbar} \sum_{i,f} |\langle\Psi_f|\Delta|\Psi_i\rangle|^2 \delta(E_f - E_i - \hbar\omega). \tag{1}$$

$\Psi_i(\Psi_f)$ are the initial (final) states of the semi-infinite solid, and $\Delta = e\hbar/2mc(\mathbf{p}\cdot\mathbf{A} + \mathbf{A}\cdot\mathbf{p})$ is the interaction Hamiltonian with the electron momentum operator $\mathbf{p}$ and the vector potential $\mathbf{A}$ of the photon field.

In the one-step model used in the present computations, Eq. (1) is manipulated into the form [5]

$$I(\mathbf{k}_\parallel, E, \hbar\omega) = -\frac{1}{\pi} \mathrm{Im}\langle\mathbf{k}_\parallel|G_2^+(E + \hbar\omega)\Delta G_1^+(E)\Delta^\dagger \times G_2^-(E + \hbar\omega)|\mathbf{k}_\parallel\rangle, \tag{2}$$

where the matrix element involves the free electron final state of momentum $\mathbf{k}_\parallel$. G_2 and G_1 denote the retarded (+) or advanced (−) one-electron Green functions at appropriate energies.

Notably, the so-called three-step model of photoemission approximates the matrix element in Eq. (1) via the *bulk* Bloch wave functions yielding for the photointensity *within* the solid [15]:

$$P(E,\omega) = \sum_{f,i} \int d^3\mathbf{k} |\langle\Psi_f^{\mathrm{bulk}}|\Delta|\Psi_i^{\mathrm{bulk}}\rangle|^2 \times A_f(E + \hbar\omega)A_i(E), \tag{3}$$

which is cast in terms of the one-particle spectral functions of the initial and final states (A_i and A_f), and the processes of transport and emission are to be considered separately. Assuming that (i) the system is strictly 2D, and (ii) the final states form a structureless continuum, Eq. (3) reduces to

$$P(E,\omega) \sim \sum_i |\langle\Psi_f^{\mathrm{bulk}}|\Delta|\Psi_i^{\mathrm{bulk}}\rangle|^2 A_i(E) \tag{4}$$

in terms of just the $A_i(E)$'s. Further, for a single band solid, one obtains

$$P(E,\omega) \sim |\langle\Psi_f^{\mathrm{bulk}}|\Delta|\Psi_i^{\mathrm{bulk}}\rangle|^2 A_i(E), \tag{5}$$

where the Fermi function on the right side is suppressed.

 0031-9007/99/83(24)/5154(4)$15.00

Brief comments on forms 1–5 are appropriate in order to highlight the underlying approximations. Since forms 3–5 ignore the presence of the surface, it is very difficult to include effects of different surface terminations [16], and the associated distortions of bulk wave function which can be quite severe. In form 4, even near an ARPES peak from a specific initial state, other states will in general contribute a background upon being broadened due to their finite lifetimes. Forms 4 and 5 ignore the structure in the final state spectrum which will be seen below to be quite significant. We emphasize that the distinctions between the processes of excitation, transport, and emission through the surface invoked by the three-step model [Eqs. (3)–(5)] are artificial since the more satisfactory one-step formula [Eq. (2)] does not admit such a decomposition.

The relevant technical details of our computations are as follows. In order to keep the problem manageable, the modulation of the lattice is neglected and the crystal structure of BISCO is assumed to be perfectly tetragonal; this still involves 30 atoms per unit cell, and a substantial extension of the earlier work on relatively simpler lattices [7,10]. The crystal potential was first obtained self-consistently within the Korringa-Kohn-Rostoker (KKR) scheme [17], and essentially yielded the well-known LDA-based band structure and Fermi surface of Bi2212 [18]; however, the actual potential used here is slightly modified in that the Bi-O pockets around the $\overline{M}$ point are lifted above the Fermi energy to account for their absence in the experimental spectra [19]. The surface is assumed to terminate in the Bi-O layer in accord with the general consensus [20] that this is an easy cleavage plane in BISCO; the incident light is assumed polarized in the (k_x, k_y) plane since the ARPES spectra of interest here seem to be insensitive to the z component A_z of the vector potential, and further, dielectric effects would in general complicate the relationship between the value of A_z inside and outside the crystal [21].

The ARPES simulations of Fig. 1 help set the stage for our discussion. As expected, the separation between the spectral features A and B in Fig. 1(a) associated with the CuO_2 plane bands increases as we go from $\overline{\Gamma}$ towards $\overline{M}$ [22]. Figures 1(b) and 1(c) show that the spectral weight of A or B depends dramatically on the values of $k_\parallel$ and photon energy $h\nu$. The weights display large changes for either peak as a function of $h\nu$ for a fixed $k_\parallel$, or as a function of $k_\parallel$ for a fixed $h\nu$. These results highlight the importance of matrix element effects in BISCO since the weights will be constant independent of $h\nu$ or $k_\parallel$ in the absence of these effects. In fact, our theoretically predicted $h\nu$ and $k_\parallel$ dependencies of spectral weights are in substantial accord with the measurements; we discuss this aspect now with reference to Figs. 2–4.

Figure 2 compares the measured and computed total spectral weights in a 500 meV energy window below E_f along the three high symmetry directions. The character-

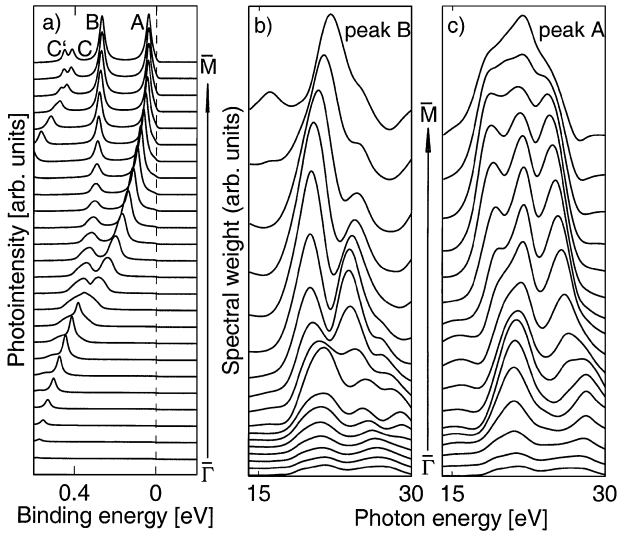

FIG. 1. (a) Simulated ARPES intensity in BISCO for $k_\parallel$ varying between $\overline{\Gamma}$ and $\overline{M}$ (bottom to top) at $h\nu = 22$ eV. (b) and (c) show computed variations in spectral weights (areas under peaks) of the two CuO_2 plane band features A and B with photon energy for different $k_\parallel$ values, based on a crystal potential without Bi-O hole pockets at $\overline{M}$. A small value of the initial and final state damping parameters is used to highlight spectral features.

istic features of the experimental data are as follows: a relatively low flat intensity along $\overline{\Gamma X}$, a steep rise along $\overline{\Gamma M}$ compared to $\overline{\Gamma Y}$, and the presence of the prominent bump around $k_\parallel \approx 0.25$ along $\overline{\Gamma Y}$. All these aspects of the data are essentially reproduced by the theory [23].

Figure 3 considers the photointensity in the (k_x, k_y) plane for two different polarizations of the incident light

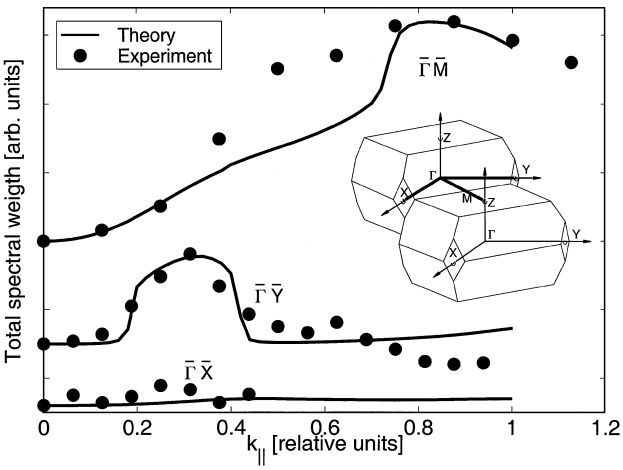

FIG. 2. Theoretical weights obtained by integrating the $h\nu = 22$ eV ARPES spectra over the binding energy range of 0–500 meV are compared with the corresponding experimental results [11]. Curves for the three symmetry lines (Brillouin zone in inset) are offset vertically for clarity; $k_\parallel$ is given in relative units such that the distance from Γ to X, Y, or M is defined to be unity for each direction. Theoretical values are normalized to match the experimental value at the maximum around $k_\parallel \approx 0.8$ in the $\overline{\Gamma M}$ curve.

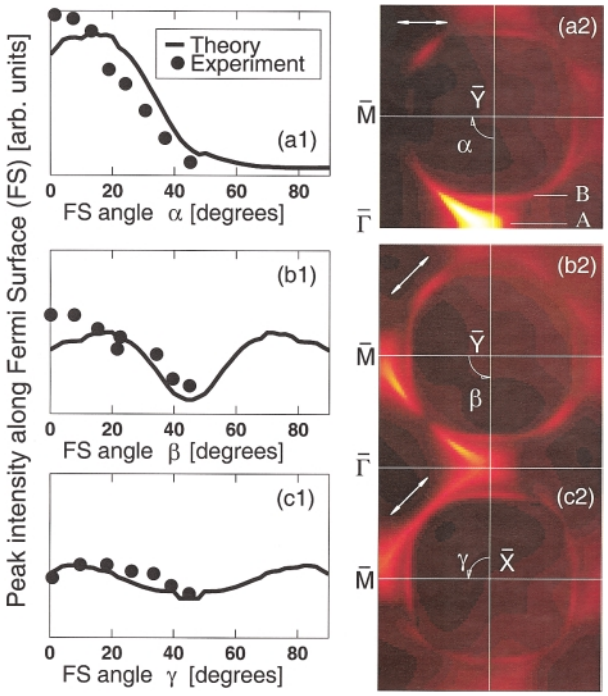

FIG. 3 (color). The color plots give simulated ARPES intensities for emission from E_f at $h\nu = 22$ eV for two different polarizations (white arrows) of the incident light. The CuO_2 plane band sheets are marked A and B. The intensity (area under peak) of the outer plane band A is shown in (a1)–(c1) as a function of the angles α, β, and γ. Experimental data after Ref. [11]. Theory normalized around $\alpha \approx 0$ as shown in (a1).

where the initial state is held fixed at E_f. The color plots give computed intensities over a dense grid of $k_\parallel$ values and display the two CuO_2 plane band sheets A and B in the band structure; these plots are representative of what could be measured in a suitably arranged constant-initial-energy angle-scanned (CIE-AS) ARPES measurement [8,24,25]. Incidentally, Figs. 3(a2)–3(c2) are not symmetric about a horizontal or vertical line through the center. In Figs. 3(b2) and 3(c2), the light is incident along the $\overline{\Gamma Y}$ direction and the figure therefore is symmetric only about this diagonal line. In Fig. 3(a2), on the other hand, the light is polarized horizontally, and the intensities are symmetric around the $\overline{\Gamma M}$ line; this symmetry becomes visible only when the figure is extended in the vertical direction to include a larger range of momenta.

The intensity associated with the outer plane band sheet A as one goes around the Fermi surface is shown in quantitative detail in Figs. 3(a1)–3(a3). Since A is generally more intense than the inner plane band B, A is presumably more relevant in connection with the experimental data near E_f. For light polarized along the horizontal direction [Fig. 3(a)], we see that the intensity is large around $\alpha = 0°$ and decreases rapidly beyond $\alpha \approx 20°$. A 45° rotation of the polarization vector [Figs. 3(b) and 3(c)] induces substantial changes in the shape and magnitude of the intensity, and the appearance of a minimum at β or $\gamma = 45°$. The experimental points in Fig. 3 are in good overall accord with the measurements, some discrepancies around α and $\beta \approx 0°$ notwithstanding. Thus quite large observed variations (nearly an order of magnitude) in the emission intensity from different parts of the Fermi surface are mainly the consequence of matrix element effects.

Finally, Fig. 4 considers the photon energy dependence of the emission intensity of the spectral feature around the $\overline{M}$ point. The theoretical curve displays a prominent peak around 22 eV and indicates clearly that the final states in BISCO possess considerable structure which is neglected in approximations of Eqs. (5) and (6), especially when the matrix element in these equations is further replaced by a constant. The experimental points which show the presence of a broad peak centered around 21 eV are in good overall agreement when we keep in mind that errors of the order of a few eV's in locating the *final states* are generally expected in the first principles band structures.

We emphasize that the agreement seen in Figs. 2–4 is robust to uncertainties inherent in such a comparison on the theoretical as well as the experimental side. The experimental weights depend on the specific energy window used in their definition, and on whether or not a suitable background is subtracted [26]. In this vein, the computed weights depend also, of course, on the specific values of the initial and final state damping parameters Σ_i'' and Σ_f''. In order to assess these effects, we have carried out extensive simulations using a variety of different values and energy dependencies of Σ_i'' and Σ_f'', in addition to varying the real part of the initial state self energy (in order to mimic correlation effects, even though the LDA framework underlies our computations), and find that the main features of the results of Figs. 2–4 are insensitive to such variations.

In summary, we have carried out extensive first-principles one-step ARPES simulations in Bi2212 wherein the photoemission process is modeled realistically by

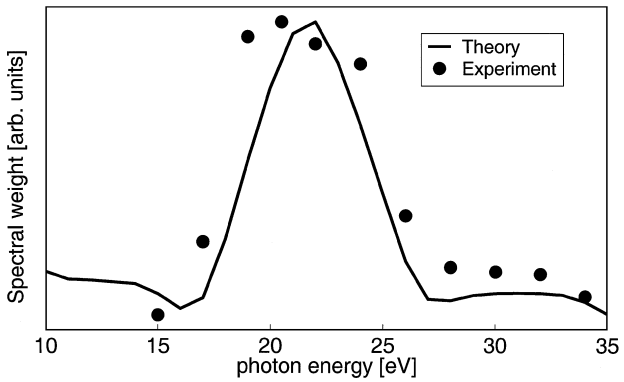

FIG. 4. Spectral weight (over a 500 meV window) of the feature at $\overline{M}$ point is compared with the corresponding experimental [11] results as a function of the photon energy. The theoretical curve is normalized to the experiment at around 21 eV.

taking into account the nature of the initial and final state crystal wave functions as well as the multiple scattering effects in the presence of a specific surface termination. We focus on the nature of the ARPES feature arising from CuO_2 plane bands, and consider in particular its spectral weight as a function of $k_\parallel$ as well as the energy and polarization of the incident photons. Large variations in the spectral weights predicted theoretically along three different high symmetry directions are in good accord with the corresponding measurements. A good agreement between theory and experiment is also seen with regard to changes in spectral weights with photon energy around the $\overline{M}$ point, as well as along the Fermi surface contours in the (k_x, k_y) plane for two different polarizations. This study shows clearly that the remarkable observed changes in the ARPES spectral weights in Bi2212 are essentially a matrix element effect and that the importance of matrix elements should be kept in mind in analyzing the ARPES spectra in high-T_c superconductors. Another notable implication of this work is that the integral (over energy) of the ARPES intensity does not yield the momentum density of the electron gas.

This work is supported by the U.S. Department of Energy under Contract No. W-31-109-ENG-38, and benefited from the allocation of supercomputer time at the NERSC and Northeastern University Advanced Scientific Computation Center (NU-ASCC).

[1] See, e.g., the collected volumes of Refs. [2–4].
[2] *Proceedings of the Conference on Spectroscopies in Novel Superconductors, Cape Cod, Massachusetts, 1997*, edited by A. Bansil, R. Markiewicz, S. Sridhar, and D. Liebenberg [J. Phys. Chem. Solids **59**, 1675–2236 (1998)].
[3] *Proceedings of the Conference on Spectroscopies in Novel Superconductors, Stanford, California, 1995*, edited by Z.-X. Shen, D. H. Liebenberg, and A. Bansil [J. Phys. Chem. Solids **56**, 1567–1974 (1995)].
[4] *Proceedings of the Conference on Spectroscopies in Novel Superconductors, Santa Fe, New Mexico, 1993*, edited by F. M. Mueller, A. Bansil, and A. J. Arko [J. Phys. Chem. Solids **54**, 1073–1470 (1993)].
[5] J. B. Pendry, Surf. Sci. **57**, 679 (1976); J. F. L. Hopkinson, J. B. Pendry, and D. J. Titterington, Comput. Phys. Commun. **19**, 69 (1981).
[6] A. Bansil and M. Lindroos, J. Phys. Chem. Solids **59**, 1879 (1998).
[7] M. Lindroos and A. Bansil, Phys. Rev. Lett. **75**, 1182 (1995).
[8] M. Lindroos and A. Bansil, Phys. Rev. Lett. **77**, 2985 (1996).
[9] K. Gofron, J. C. Campuzano, A. A. Abrikosov, M. Lindroos, A. Bansil, H. Ding, and B. Dabrowski, Phys. Rev. Lett. **73**, 3302 (1994).
[10] A. Bansil and M. Lindroos, J. Phys. Chem. Solids **56**, 1855 (1995).
[11] J. C. Campuzano and H. Ding (private communication); data based in part on results of Ding *et al.* [Phys. Rev. Lett. **76**, 1533 (1996)].
[12] As an operational definition, by "matrix element effects" we mean the effect of approximating the true spectral photointensity of, say, Eq. (2) by the bulk initial state spectral density function $A_i(E)$.
[13] P. W. Anderson and Y. Ren in, *High Temperature Superconductivity*, edited by K. S. Bedell *et al.* (Addison-Wesley, Redwood City, California, 1990).
[14] N. W. Ashcroft and W. I. Schaich, Phys. Rev. B **3**, 2452 (1971).
[15] C. Kunz in *Photoemission in Solids II*, edited by L. Ley and M. Cardona (Springer-Verlag, Berlin, 1979), p. 313.
[16] M. Lindroos *et al.*, Physica (Amsterdam) **212C**, 347 (1993).
[17] A. Bansil, S. Kaprzyk, and J. Tobola, in MRS Symposium Proceedings No. 253 (Materials Research Society, Pittsburgh, 1992), p. 505; A. Bansil and S. Kaprzyk, Phys. Rev. B **43**, 10335 (1991); S. Kaprzyk and A. Bansil, Phys. Rev. B **42**, 7358 (1990); A. Bansil, S. Kaprzyk, P. E. Mijnarends, and J. Tobola, Phys. Rev. B **60**, 13 396 (1999).
[18] S. Massida, J. Yu, and A. J. Freeman, Physica (Amsterdam) **152C**, 251 (1988); H. Krakauer and W. E. Pickett, Phys. Rev. Lett. **60**, 1665 (1988); M. S. Hybertsen and L. F. Mattheiss, Phys. Rev. Lett. **60**, 1661 (1988).
[19] Although the ARPES data from BISCO suggest the absence of Bi-O pockets around $\overline{M}$, the conclusions of this article are insensitive to whether or not this is so.
[20] See, e.g., D. M. Ori, A. Goldoni, U. del Pennino, and F. Parmigiani, Phys. Rev. B **52**, 3727 (1995).
[21] See, e.g., A. Gerlach, R. Matzdorf, and A. Goldmann, Phys. Rev. B **58**, 10 969 (1998).
[22] Experimental spectra do not obviously indicate the presence of a feature like C or C' close to E_f. However, the location of C, C' is quite sensitive to the crystal potential in the Bi-O planes which has been modified somewhat in these simulations to move the Bi-O pockets above E_f.
[23] The discrepancy in Fig. 2 between 0.4–0.8 along ΓM is related to the structures C and C' in theory and is not considered serious; see also Ref. [22] above.
[24] N. L. Saini *et al.*, Phys. Rev. Lett. **79**, 3467 (1997).
[25] The finer details (as in the data of Ref. [24]) associated with modulations and possible stripe phases are, of course, not reproduced in the color plots of Fig. 3 which assume a perfect tetragonal lattice.
[26] Although experimental data after Ref. [11] is used in Figs. 2–4, results from various groups are similar; see, e.g., Loeser *et al.* [27]; Chuang *et al.* [28]; Saini *et al.* [24].
[27] A. G. Loeser *et al.*, Phys. Rev. B **56**, 14185 (1997).
[28] Y.-D. Chuang *et al.* (preprint cond-mat/9904050).